

Hydrogen Recombination with Multilevel atoms

Soma De¹, E. Baron^{1,2}, P. H. Hauschildt³

¹*Homer L. Dodge Dept. of Physics and Astronomy, University of Oklahoma, Norman, OK 73019, USA*

²*Computational Research Division, Lawrence Berkeley National Laboratory, MS 50F-1650, 1 Cyclotron Rd, Berkeley, CA 94720 USA*

³*Hamburger Sternwarte, Gojenbergsweg 112, 21029 Hamburg, Germany*

28 March 2022

ABSTRACT

Hydrogen recombination is one of the most important atomic processes in many astrophysical objects such as Type II supernova (SN II) atmospheres, the high redshift universe during the cosmological recombination era, and H II regions in the interstellar medium. Accurate predictions of the ionization fraction can be quite different from those given by a simple solution if one takes into account many angular momentum sub-states, non-resonant processes, and calculates the rates of all atomic processes from the solution of the radiative transfer equation instead of using a Planck function under the assumption of thermal equilibrium. We use the general purpose model atmosphere code PHOENIX 1D to compare how the fundamental probabilities such as the photo-ionization probability, the escape probability, and the collisional de-excitation probability are affected by the presence of other metals in the environment, multiple angular momentum sub-states, and non-resonant processes. Our comparisons are based on a model of SN 1999em, a SNe Type II, 20 days after its explosion.

Key words: Supernova: hydrogen recombination

1 INTRODUCTION

Hydrogen recombination plays a very important role in many astrophysical phenomena such as Type II supernovae, the interstellar medium, and cosmic recombination.

Time-dependent recombination has been studied for the case of cosmological recombination (Zeldovich et al. 1969; Peebles 1968) and for supernovae (Utrobin & Chugai 2005; Dessart & Hillier 2008; De, Baron & Hauschildt 2009). In supernovae this occurs when the hydrogen recombination time-scale becomes comparable to the age of the supernova. This effect is found to be dominant in the early epochs of the supernova's evolution (De et al. 2009). At later times, however, effects due to multi-level atom effects (the importance of having many angular momentum sub-states) become more important than time-dependent phenomena. De et al. (2009) discussed how the effective recombination timescale can be different based on time-dependent rate equations using different hydrogen atom models. The primary goal of De et al. (2009) was to determine the epoch in the lifetime of a supernova (during the photospheric phase) where time-dependence in the rate equations is most important. In doing so we found that at later times model atoms with significantly more energy levels (that is additional angular-momentum sub-states) have a strong effect in determining the effective recombination time-scale. This issue is also important for applications other than supernovae. In fact, considering more complete atomic models is important to correctly estimate the electron density and recover subtle features in the spectra. Here, we study multi-level atomic systems for hydrogen alone using a non-LTE treatment which could alter the hydrogen ionization fraction and therefore produce a different temperature structure.

Cosmological recombination codes such as RECFAST (Seager et al. 1999, 2000;

Wong et al. 2008) and RICO (Fendt et al. 2009) that deal with cosmological recombination and solve for the free electron fraction as a function of redshift do an excellent job. Nevertheless there are assumptions about Saha equilibrium between higher angular momentum states. Grin & Hirata (2010) have presented their recombination code RECSPARSE which is a highly detailed calculation but still uses the Sobolev approximation for line calculations. Recently the cosmological recombination problem has been revisited by several authors, paying special attention to possibly neglected atomic physics effects. The processes studied have included two-photon decays in H I and He I (Dubrovich & Grachev 2005; Wong & Scott 2007; Chluba & Sunyaev 2008; Hirata 2008; Karshenboim & Ivanov 2008; Hirata & Switzer 2008), H I continuum absorption of the He I $\lambda 584$ line photons (Switzer & Hirata 2008a,b; Rubiño-Martín et al. 2008; Kholupenko et al. 2007), stimulated two-photon decays and two-photon absorption (Hirata 2008; Chluba & Sunyaev 2006; Karshenboim & Ivanov 2008), Raman scattering (Hirata 2008; Hirata & Switzer 2008), a more complete set of angular momentum substates (Grin & Hirata 2010), and forbidden transitions in He I (Wong & Scott 2007; Switzer & Hirata 2008a,b; Rubiño-Martín et al. 2008). Hirata & Forbes (2009) studied the effects of partial frequency redistribution, line blanketing, and time-dependence in Ly- α , but even then made use of the Sobolev approximation. Here we resolve all line profiles in the co-moving frame and accurately treat line blanketing. We assume complete redistribution for the line profiles.

We focus primarily on estimating the photo-ionization rate, the escape probability, and the collisional de-excitation rate. We show how these rates depend on the hydrogen model atom used and we also study the effects of the presence of metals on the results. These different rates ultimately lead to variations in the hydrogen ionization fraction. We also examine when the 2γ process plays the most significant role in controlling hydrogen recombination.

In § 2, we outline the theoretical framework relating the photo-ionization rate,

collisional de-excitation rate, and escape probability to the effective hydrogen recombination time. In § 3, we describe our approach and different test systems that we study. In § 4 we present our results. In § 5, we state our conclusions and describe a possible framework for future work.

2 THEORETICAL FRAMEWORK FOR HYDROGEN RECOMBINATION

The ionization fraction for hydrogen is defined as

$$f_{\text{H}} = \frac{n_{\text{H}^+}}{n_{\text{H}^+} + n_{\text{H}}} . \quad (1)$$

For any system the ionization fraction depends on the net recombination rate in the system. For a system in LTE, the ionization fraction can be calculated using the Saha equation with knowledge of the electron density and temperature. On the other hand, for systems not in LTE, it is important to solve the radiative transfer equation and the rate equations simultaneously. The recombination rate of a system is dependent on the number of angular momentum sub-states of the system and also on the presence of other elements in the environment that can contribute to the free electron density. The recombination process in a system is determined by the net rate of photo-ionization and its inverse process (recombination) which are modified due to line transitions. The effectiveness (towards recombination) of a resonant transition depends on the escape probability of the line. Also there are non-radiative transitions that take place such as the collisional de-excitation of electrons to lower energy levels. In addition to these there is the downward 2γ process that connects states of the same parity while the corresponding upward transition rate is very low. Therefore it is important to study all these quantities to determine the correct nature of recombination. We investigate the 2γ process, the photo-ionization rate, the escape probability and the collisional de-excitation rates of systems with different

hydrogen atom models and metallicities of the environment. We denote P_n as the photo-ionization rate from a state with index n (which is not its principal quantum number). Similarly, we define the escape probability as β_{n1} which is the escape probability for the resonant line photon between the level $1s$ and the level characterized by index n . The collisional de-excitation rate is defined as the rate of de-excitation of the electron from level n into the $1s$ state. The analytical evaluation of each of these quantities is possible if the system is in LTE or if the system has a model atom which has just a very few angular momentum sub-states. But for a system with many angular momentum sub states (we consider 921 bound levels for hydrogen) and in the presence of metals, it is necessary to evaluate these quantities numerically from a consistent solution of the radiative transfer equation and the rate equations.

The results presented in this paper are obtained by simultaneously solving the coupled radiative transfer equation and rate equations. The rate equations use multi-level atoms including a large set of line and continuum transitions. The upward radiative rate ($i \rightarrow j$) is given as $n_i R_{ij}$ where i is a bound state and j can be a bound or continuum state. n_i is the population for level i . R_{ij} is given as (Mihalas 1978):

$$R_{ij} = 4\pi \int_{\nu_0}^{\infty} \alpha_{ij}(\nu) (h\nu)^{-1} J_{\nu} d\nu . \quad (2)$$

Similarly the downward rate ($j \rightarrow i$) is calculated as $n_j (\frac{n_i}{n_j})^* R_{ji}$ where R_{ji} is:

$$R_{ji} = 4\pi \int_{\nu_0}^{\infty} \alpha_{ij}(\nu) (h\nu)^{-1} \left[\left(\frac{2h\nu^3}{c^2} \right) + J_{\nu} \right] e^{-\frac{h\nu}{kT}} d\nu . \quad (3)$$

In the above equations J_{ν} is the angle averaged radiation intensity at frequency ν . T is the temperature, k is Boltzmann's constant, α_{ij} is the photo-ionization cross section for the $i \rightarrow j$ transition, and ν_0 is the threshold frequency. The level populations denoted with (*) are the equilibrium values as defined by Mihalas (1978). In our calculations the Sobolev approximation has not been used. In order to compare our

results with others we plot the values of the Sobolev escape probability. All the level populations were calculated without assuming the Sobolev approximation.

Below we give the equations that define P_n , β_{n1} (Mihalas 1978). Firstly,

$$P_n = |n_n R_{n\kappa} - n_\kappa \left(\frac{n_n}{n_\kappa}\right)^* R_{\kappa n}|, \quad (4)$$

where κ stands for the continuum level.

The escape probability β_{n1} is defined using the Sobolev escape probability as

$$\beta_{n1} = \frac{1 - e^{-\eta_{n1}}}{\eta_{n1}}, \quad (5)$$

$$\eta_{n1} = \frac{\pi e^2}{m_e c} f_{n1} \lambda_{n1} t \left(n_1 - \frac{g_1}{g_n} n_n \right), \quad (6)$$

where f_{n1} is the oscillator strength of the line between excited level n and the ground state. n_1 and n_n are the number densities of the ground state and the excited state referred by index n , respectively. λ_{n1} is the wavelength of the line, t is the time since explosion in seconds. g_n is the degeneracy of level n and $\frac{g_1}{g_2} \sim \frac{1}{n^2}$ (Mihalas 1978). In § 3 we discuss our approach to quantify the photo-ionization rate, the escape probability, and the collisional de-excitation rate.

3 VARIATION OF HYDROGEN MODEL ATOMS AND COMPOSITION

3.1 Description of the test systems

To set up the physical structure of each system we use the density profile and luminosity from a full NLTE calculation of a model atmosphere in homologous expansion, with a power-law density profile $\rho \propto v^{-7}$, 20 days after explosion, which is a reasonable fit to observed spectra of SN 1999em at that epoch. This underlying density profile and the total bolometric luminosity in the observer's frame are chosen to be representative of the conditions in SNe IIP near maximum light. Give this structure

we use our general purpose model atmosphere code PHOENIX 1D to solve for the new temperature structure and level populations under the new conditions (such as the hydrogen model atom and the presence of other metals). The initial model of SN 1999em at 20 days after explosion was generated using a 31 level hydrogen model atom and solar metals were included. We call this starting model our base model. Our base model was generated treating hydrogen and other elements in NLTE. The details of our radiative transfer code are described in Hauschildt & Baron (1999; 2004 and references therein). The transfer equation and the rate equations were all time independent for the base model. The physical properties related to our base model are given in Table 1.

Now we define the different systems that we experimented upon to study the behavior of the physical quantities affecting the recombination rate. For convenience, we name the different systems in the following way. We refer to Model A as the system which has only hydrogen and the hydrogen model atom in this case has just 4 bound states ($1s, 2s, 2p_{\frac{1}{2}}, 2p_{\frac{3}{2}}$) and 4 lines that couple those states. Model C is the same as Model A, except it has a solar composition of metals present in the system in addition to hydrogen and all the other metals are treated in LTE. Model B has only hydrogen in the system but the hydrogen model atom has 921 bound levels and 995 lines that couple the bound states. Model D is the same as Model B except this has metals present and the metals are treated in LTE as in Model C. The LTE treatment of metals was chosen to reduce computing time and in a hydrogen rich environment the main role that metals play in continuum processes is to be a source of additional electrons. We did not focus on how their atomic structure affects hydrogen recombination.

For Models A and C, there are primarily three major processes considered that

couple the bound states:

$$H_{1s} + \gamma \rightarrow e^- + H^+ ;$$

$$H_{1s} + \gamma \leftrightarrow H_{2p} ;$$

$$H_{2s} \rightarrow H_{1s} + 2\gamma.$$

In addition to this the $1s$ and $2p$ states are coupled by spontaneous transitions. In models B and D the atomic line data were taken from Kurucz (1995).

4 RESULTS

We study the rates and the resulting hydrogen ionization fraction, f_H , among the four different systems that have been described in § 3. These different systems can have different ionization fractions primarily because the solution of the transfer equation and the resulting temperature structure will be different than in the base model. The models that have metals (Models C and D) are expected to have temperature structures similar to the base model. The 4-level hydrogen atom model without metals is likely to have a different temperature structure than the base model. These differences could be subtle but important enough to change to the hydrogen ionization fraction. In our results we have also studied whether the 2γ process has a significant effect on the recombination time scale or the resulting ionization level or the consequent temperature structure of the system.

We define τ_{std} as the optical depth corresponding to the continuum opacity at 500 nm. We classify our results depending on whether the temperature structure was held fixed at the base model value or was allowed to reach radiative equilibrium under the particular assumptions of each case, in order to isolate the effect of temperature change on the level populations and the hydrogen ionization fraction.

Table 1. Physical characteristics from our base model.

τ	ρ (g cm ⁻³)	R (cm)	v (km s ⁻¹)	T (K)	n_e (cm ⁻³)	μ
9.897E-05	1.823E-15	2.454E+15	14200.00	3157.61	99464.3	1.34
3.626	3.084E-13	1.242E+15	7187.50	7345.20	1.079E+11	0.75
804.480	6.533E-12	4.104E+14	2375.00	26155.8	2.97E+12	0.67

The columns give various quantities as a function of optical depth. ρ is the mass density, R is the radius, v is the velocity, T is the matter temperature, n_e is the electron density, and μ is the mean molecular weight.

4.1 Metal-rich Models

We first discuss our results for the models where the composition included metals. We treat helium and metals in LTE. Hydrogen is always treated in NLTE. Recall that these systems are termed Models C and D for the 4-level and 921-level hydrogen atom models, respectively. Figure 1 shows the hydrogen ionization fraction for Models C and D. There is a significant change in the hydrogen ionization level, f_H , between Models C and D. The quantity f_H decreases in the multi-level atom case in the lower optical depth regime. For $\tau_{std} > 0.1$ the ionization levels among Models C and D are not very different. The quantitative difference is also tabulated in Table 2 which shows the physical parameters for Models C and D when the 2γ process was or was not included. The reduction in f_H due to additional angular momentum sub-states was about a factor of 3 at an optical depth of about $\tau_{std} \sim 10^{-4}$ (when the 2γ process was included in both the models). The difference in f_H decreases as the optical depth increases. In metal-rich systems, (Models C and D), the exclusion of the 2γ process did not seem to have any significant effect for almost all optical depths of interest.

Figure 2 displays the net photo-ionization rate from any bound state of the hydrogen atom, P_n , for the levels $2p_{1/2}$ and $2p_{3/2}$ for Model C. The profile of P_n for Model C is not monotonic, but there is an overall trend to increase with optical depth, τ_{std} . This increase in P_n is expected due to the fact that photo-ionization dominates over recombination at higher optical depths due to higher temperatures. Figure 3 shows

the net photo-ionization rate as a function of wave number of each energy level for Model D. Different panels show different τ_{std} regimes. The P_n values increase with increasing τ_{std} for a given energy level. Also the net photo-ionization rate does not change significantly with the change in the energy level of the bound state. There is a drop in the P_n profile at energy levels very close to the continuum. This may be due to the fact that very high energy bound states are not really distinguished from the continuum, therefore the *net* photo-ionization rate falls off.

For the calculation of the escape probability (defined as the probability for the escape of the resonant line connecting the ground state and higher energy bound state), are shown in Figures 4–5. Figure 4 shows the escape probability for Model C, for levels $2p_{1/2}$ and $2p_{3/2}$. The escape probability for Model C decreases with increasing optical depth and also decreases with decreasing energy of the bound state. For Model D (Figure 5) the escape probability increases with increasing energy of the bound state. Also the escape probability decreases very slowly with the increase in optical depth for Model D, similar to that in Model C. The apparent difference between Models C and D is that the escape probability decreased for a higher energy level in Model C as opposed to case D where the escape probability increased with the increased energy of the bound state. For Model C, the levels in question are both $2p$ states and in Model D for those two $2p$ states we also find a slight reduction in the escape probability with increasing energy of the bound state.

The reduction in the escape probability as a function of optical depth can be explained from Eq. 6. At higher optical depths (for a given excited state), when n_n , the population of the excited state increases, this results in a decrease in the quantity η_{n1} . Following the decrease in η_{n1} , the escape probability β_{n1} decreases. On the other hand at a given optical depth with increasing energy of the bound state, the escape probability increases. At a given τ_{std} , for an increase in the bound state energy, n_n decreases and λ_{n1} decreases, hence the overall effect almost always is to decrease β_{n1} .

Figure 6 shows the collisional de-excitation rate (which is the collisional de-excitation coefficient q_e times the free electron density n_e) for Model C. In this Model there is an increase in the collisional de-excitation rate with increasing optical depth. For Model D, the collisional de-excitation rate follows a similar pattern. The increase in the free electron density with increasing τ_{std} explains the increased collisional de-excitation rate with τ_{std} . To summarize, the characteristics of the metal-rich Models C and D, 1) the ionization fraction decreases for a multi-level hydrogen atom compared to a 4-level hydrogen atom. 2) The net photo-ionization rate increases with optical depth for a given bound state. The photo-ionization rate also does not change significantly at a given τ_{std} as the energy of the bound state increases. 3) The escape probability decreases with increasing τ_{std} , although this decrease is very small. The escape probability increases with increasing energy of the bound state except for the case of the $2p$ states. 4) The collisional rate increases with increasing optical depth. Also for the multi-level case the rate is close to the equilibrium value. 5) The 2γ process did not seem to have any significant effects in Models C and D.

4.2 Metal-deficient Models

In this section we focus on Models A and B. Recall that Models A and B are models where the atmosphere consists of pure hydrogen. Hydrogen was treated in NLTE in these models. In Model A, we use a 4-level hydrogen atom and in Model B, we use a hydrogen atom model with 921 energy levels. We also study how the 2γ process affects these systems when the environment is metal-free. Figure 7 displays the ionization fraction for Models A and B. Interestingly f_H does not change significantly between Models A and B. This is quite different when compared to Models C and D. Table 2 shows the changes due to the 2γ process. For Model A, at low optical depths ($\tau_{std} \sim 10^{-4}$) turning on the 2γ process produces about a 20% change in the free electron

density, but for $\tau_{std} \gtrsim 10^{-3}$ no significant change is seen. For Model B, there is a significant reduction in the free electron density due to the inclusion of the 2γ process. The electron density is 5 times higher with the inclusion of the 2γ process in case B, at low optical depths, $\tau_{std} \sim 10^{-4}$. For higher optical depths, there is no significant effect due to the 2γ process. The decrease in the free electron density due to the 2γ process is expected since the upward process is suppressed by a factor of $1/137$. The change is especially noticeable in Model B. It is at a fairly low optical depth where the change in the rates observed but this is also the optical depth where the optical depth of the Balmer line is high (De et al. 2009). This wavelength regime is similar to what is described in De et al. (2009).

The net photo-ionization rate (P_n) does not change significantly between different bound states in both Models A and B (see Figures 8 and 9). Although in the multi-level case (case B), P_n increases by almost a factor of 10 from the lowest energy bound state to the higher energy bound states (except for the states very close to the continuum) at low optical depths ($\tau_{std} < 0.01$). Figures 10 and 11 show the escape probability for Models A and B respectively. The trend is very similar to that of Models C and D. The collisional de-excitation rate increases with increasing optical depths in both the Models C and D

To summarize: our findings on Models A and B (pure hydrogen models) 1) For most optical depth regimes, the basic trend in the rates is similar to Models C and D. 2) The 2γ process seems to have a significant effect in both Model A and B (at lower τ_{std}). The effect is much larger for Model B. This effect was not seen in Models C and D.

We observe the following, for almost all optical depths,

$$\begin{aligned} P_n(A) &> P_n(C); \\ \beta_{n1}(A) &< \beta_{n1}(C); \end{aligned}$$

$$n_e q_{n1}(A) < n_e q_{n1}(C).$$

For Models B and D,

$$P_n(B) < P_n(D) \quad (\tau < 0.01);$$

$$\beta_{n1}(B) \approx \beta_{n1}(D);$$

$$n_e q_{n1}(B) < n_e q_{n1}(D) \quad (\tau < 0.01).$$

The difference in the profiles of P_n , β_{n1} and $n_e q_{n1}$ between Model A (or B) and Model C (or D) can be attributed to their different temperature profiles.

4.3 Metal-deficient case without temperature corrections

In our previous Models A–D, we allowed the system to reach radiative equilibrium for each assumption. It is useful to hold the temperature structure fixed and just examine the changes that are due to the variation in the compositions and model atoms. In the fixed temperature structure case we do not find a large difference as compared to the radiative equilibrium case. The differences, compared to the radiative equilibrium case occurs in the optical depth region $10^{-3} < \tau < 10^{-2}$. There is a slight suppression in the ionization fraction for Model B compared to Model A. The other rates are nearly identical.

5 DISCUSSION

The primary motivation for this paper was to investigate how the multi-level structure of the hydrogen model atom affects the hydrogen ionization fraction as well as the photo-ionization, escape, and collisional de-excitation rates. We also investigated if the the metals in the environment or if the 2γ process plays a significant role in the recombination process of the system. We find that a multi-level hydrogen atom structure, or in other words a more complete set of energy levels to be important

Table 2. Physical characteristics from four different models, under radiative equilibrium

Model Name	Type	τ	T (K)	N_e (cm $^{-3}$)	μ
A	4 level	0.00016	2820.75	105236.	1.01
		0.02343	4011.17	9.999E+07	1.01
		3.61	7564.24	2.351E+11	0.54
		1104.90	27565.10	3.903E+12	0.50
A'	4 level, no 2γ process	0.00016	2820.61	121450.	1.01
		0.02345	4011.18	9.999E+07	1.01
		3.61	7564.29	2.351E+11	0.54
		1106.10	26840.2	3.9035E+12	0.50
B	921 level	0.00016	2801.08	3.946E+5	1.01
		0.0272	4547.80	2.981E+8	1.01
		1.794	6779.06	1.087E+11	0.57
		1181.	20462.42	3.893E+12	0.50
B'	921 level, no 2γ process	0.000157	2826.28	6.709E+4	1.01
		0.02705	4547.69	2.983E+08	1.01
		1.794	6778.83	1.0864E+11	0.57
		1181	20462.42	3.801E+12	0.50
C	4 level, metal-rich environment	0.00023	3564.79	271828.	1.26
		4.91280	7584.85	1.260E+11	0.68
		867.030	26365.40	3.162E+12	0.625
C'	4 level, metal rich environment no 2γ process	0.00023	3564.78	271808.	1.26
		4.91270	7584.84	1.260E+11	0.68
		867.900	26243.10	3.160E+12	0.625
D	921 level, metal rich environment	0.00011	3099.54	84640.4	1.26
		0.98338	6337.20	4.254E+10	0.98
		863.240	26109.80	3.156E+12	0.63
D'	921 level, metal rich environment no 2γ process	0.00011	3099.46	84638.0	1.26
		0.98373	6337.44	4.256E+10	0.98
		863.080	26113.50	3.156E+12	0.63

in determining the ionization profile of the system. Recently, Grin & Hirata (2010) studied the effects of including a more complete set of angular momentum substates in the study of cosmological recombination and also found that including more substates to be important. The need to have a more complete set of bound states in the hydrogen atom is found to be more important in a metal-rich environment. This is because of the fact that recombination is more effective in a multi-level framework. When there is a source of additional free electrons (such as metals), the suppression

in f_H is larger than in pure hydrogen models. This is merely due to the fact that the larger free electron density drives recombination, thus it is very important to use multi-level hydrogen atoms especially in realistic environments with solar compositions.

The enhancement of recombination is indicated by the increasing escape probability for the higher bound states (for both Models B and D). This is also reinforced by the almost constant photo-ionization rate over different energy bound states.

The importance of the 2γ process is seen in the 4-level pure hydrogen case (Model A) as only a small reduction in the free electron density. In Model B, the reduction in the free electron density due to the inclusion of the 2γ process is much larger. There was not any significant effect due to the 2γ process in the solar composition Models. The larger change in Model B (at lower τ_{std}) can be explained from Figure 12. At low optical depths the relative population of the ground state to the first excited state is displayed. For the metal-free Models (A and B) the ratio $\frac{n_1}{n_2}$ is not very high and about 4.0 for Model B. Thus in Model B, the first excited state population is not significantly lower than the ground state population. The relative first excited state population is much lower in Models C and D (where the ratio is around $10^4 - 10^5$ at similar τ_{std}). The high level population of the first excited state (for Model B) increases the importance of the 2γ process, due to the higher number of available electrons that can recombine into the ground state and the upward transition probability for this non-resonant process being low, thus the recombination obtained is more effective. We find that it is essential to incorporate both multi-level atoms and the 2γ process. Our primary purpose was to do a simple calculation to emphasize the important factors in determining the recombination of hydrogen at typical free electron densities found in Type II supernova atmospheres. Our results show that it is important to incorporate 2γ transitions and multiple angular momentum sub-states at low optical depths where the free electron density is small (typically

$\sim 10^5 \text{ cm}^{-3}$) and is also typical of the free electron density during the epoch of cosmological recombination (Peebles 1968). In H II regions the electron density is much lower making the hydrogen recombination time scale rise. Therefore accurate treatment of hydrogen recombination is important in all of these scenarios. In the future we plan to investigate hydrogen recombination in the context of cosmological recombination epoch.

ACKNOWLEDGMENTS

We thank the anonymous referee for helpful comments which significantly improved the presentation of this work. This work was supported in part by NSF grant AST-0707704, Department of Energy Award Number DE-FG02-07ER41517, and by SFB grant 676 from the DFG. This research used resources of the National Energy Research Scientific Computing Center (NERSC), which is supported by the Office of Science of the U.S. Department of Energy under Contract No. DE-AC02-05CH11231; and the Höchstleistungs Rechenzentrum Nord (HLRN). We thank both these institutions for a generous allocation of computer time.

REFERENCES

- Chluba J., Sunyaev R. A., 2006, *A&A*, 446, 39
Chluba J., Sunyaev R. A., 2008, *A&A*, 480, 629
De S., Baron E., Hauschildt P. H., 2009, *MNRAS*, 401, 2081
Dessart L., Hillier D. J., 2008, *MNRAS*, 383, 57
Dubrovich V. K., Grachev S. I., 2005, *Astronomy Letters*, 31, 359
Fendt W. A., Chluba J., Rubiño-Martín J. A., Wandelt B. D., 2009, *ApJS*, 181, 627
Grin D., Hirata C. M., 2010, *Phys Rev D*, 81, 083005
Hauschildt P. H., Baron E., 1999, *J. Comp. Applied Math.*, 109, 41

- Hauschildt P. H., Baron E., 2004, *Mitteilungen der Mathematischen Gesellschaft in Hamburg*, 24, 1
- Hirata C. M., 2008, *Phys. Rev. D*, 78, 023001
- Hirata C. M., Forbes J., 2009, *Phys. Rev. D*, 80, 023001
- Hirata C. M., Switzer E. R., 2008, *Phys. Rev. D*, 77, 083007
- Karshenboim S. G., Ivanov V. G., 2008, *Astronomy Letters*, 34, 289
- Kholupenko E. E., Ivanchik A. V., Varshalovich D. A., 2007, *MNRAS*, 378, L39
- Kurucz R. L., 1995, *Highlights of Astronomy*, 10, 579
- Mihalas D., 1978, *Stellar Atmospheres*. W. H. Freeman, New York
- Peebles P. J. E., 1968, *ApJ*, 153, 1
- Rubiño-Martín J. A., Chluba J., Sunyaev R. A., 2008, *A&A*, 485, 377
- Seager S., Sasselov D. D., Scott D., 1999, *ApJ*, 523, L1
- Seager S., Sasselov D. D., Scott D., 2000, *ApJS*, 128, 407
- Switzer E. R., Hirata C. M., 2008a, *Phys. Rev. D*, 77, 083006
- Switzer E. R., Hirata C. M., 2008b, *Phys. Rev. D*, 77, 083008
- Utrobin V. P., Chugai N. N., 2005, *A&A*, 441, 271
- Wong W. Y., Moss A., Scott D., 2008, *MNRAS*, 386, 1023
- Wong W. Y., Scott D., 2007, *MNRAS*, 375, 1441
- Zeldovich Y. B., Kurt V. G., Syunyaev R. A., 1969, *Soviet Journal of Experimental and Theoretical Physics*, 28, 146

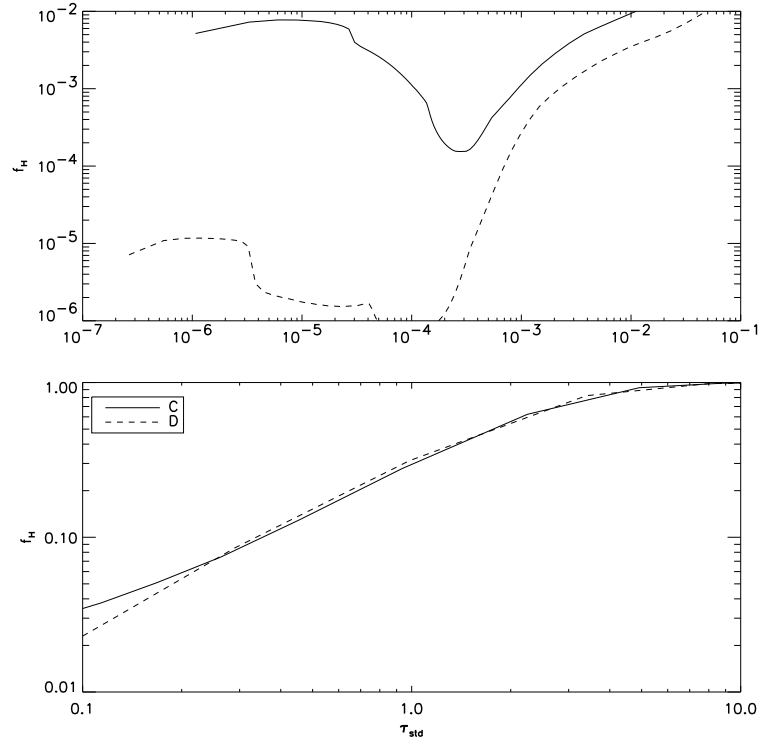


Figure 1. Comparison of the hydrogen ionization fraction found using the 4 level (C) and 921-level (D) model atoms in a metal-rich environment. The upper panel shows the lower optical depth regime while the lower panel shows the higher optical depth regime. We define τ_{std} as the optical depth corresponding to the continuum opacity at 500 nm.

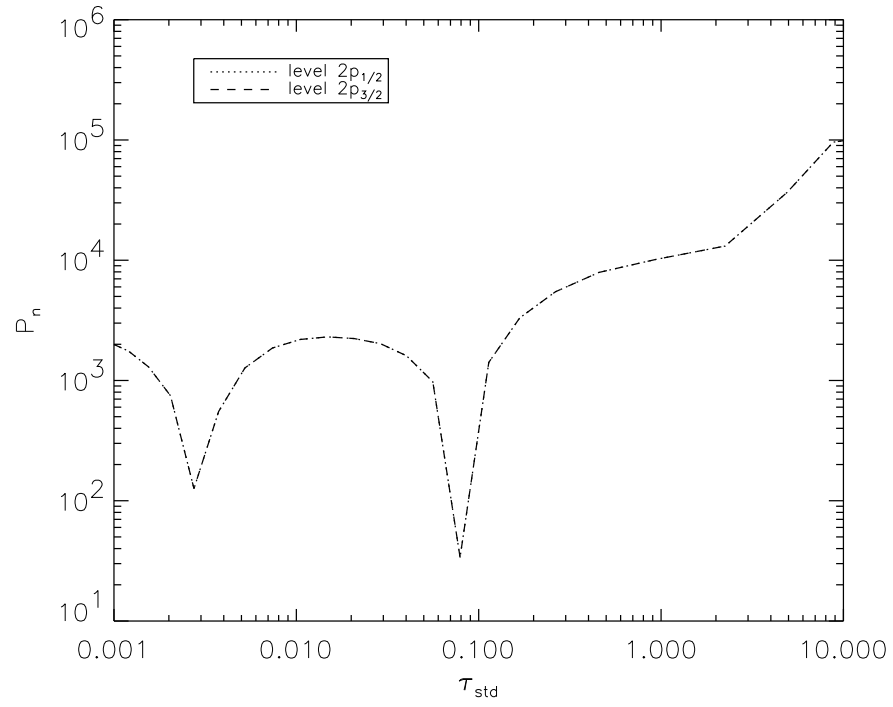


Figure 2. Photo-ionization rates of the $2p$ states versus optical depth for Model C.

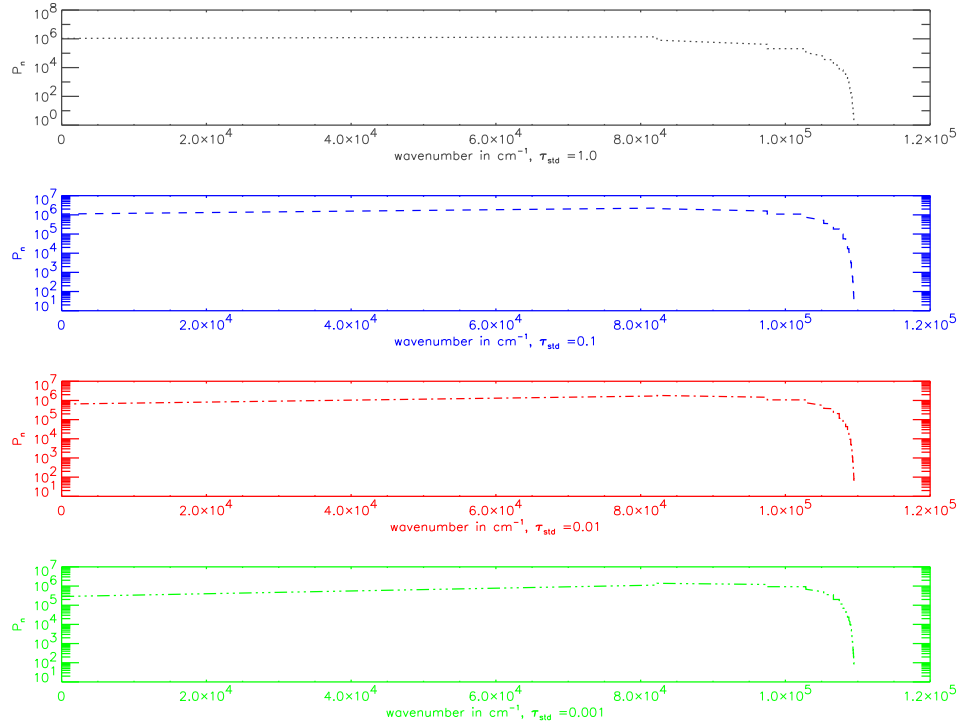


Figure 3. Photo-ionization rates versus energy level for Model D at different optical depths. Each panel shows a particular optical depth.

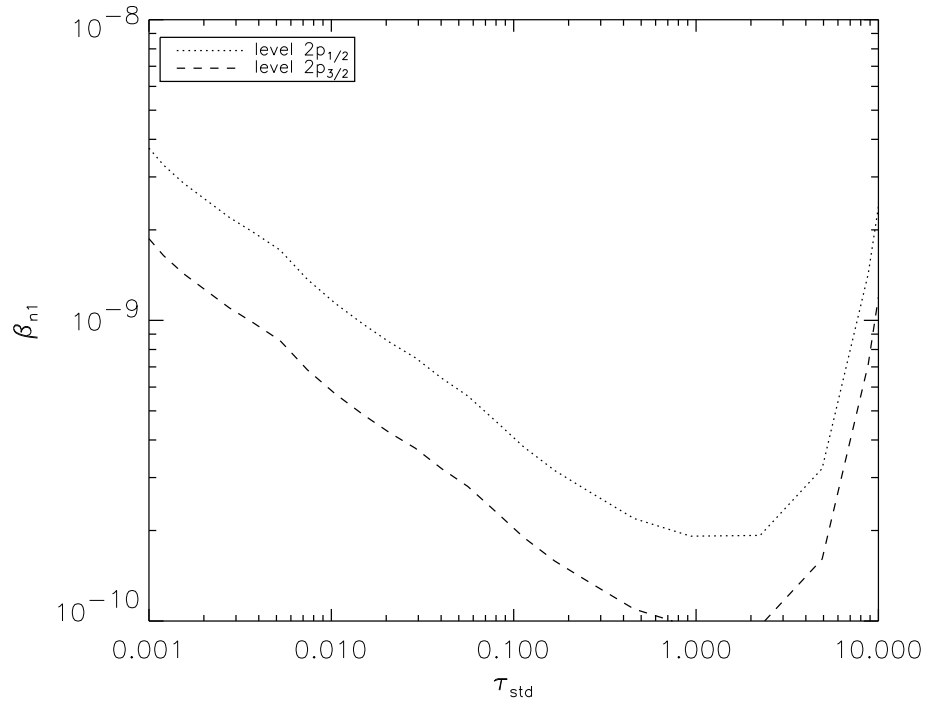


Figure 4. Escape probability versus optical depth for the 2p states for Model C.

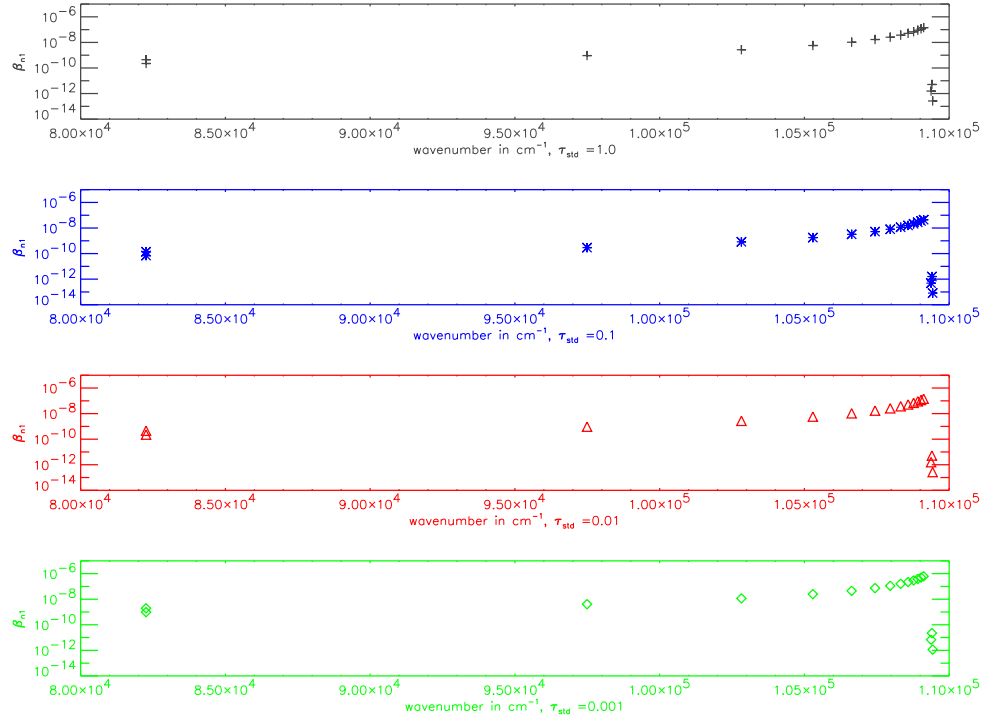


Figure 5. Escape probability versus energy levels for Model D at different optical depths. Each panel shows a particular optical depth.

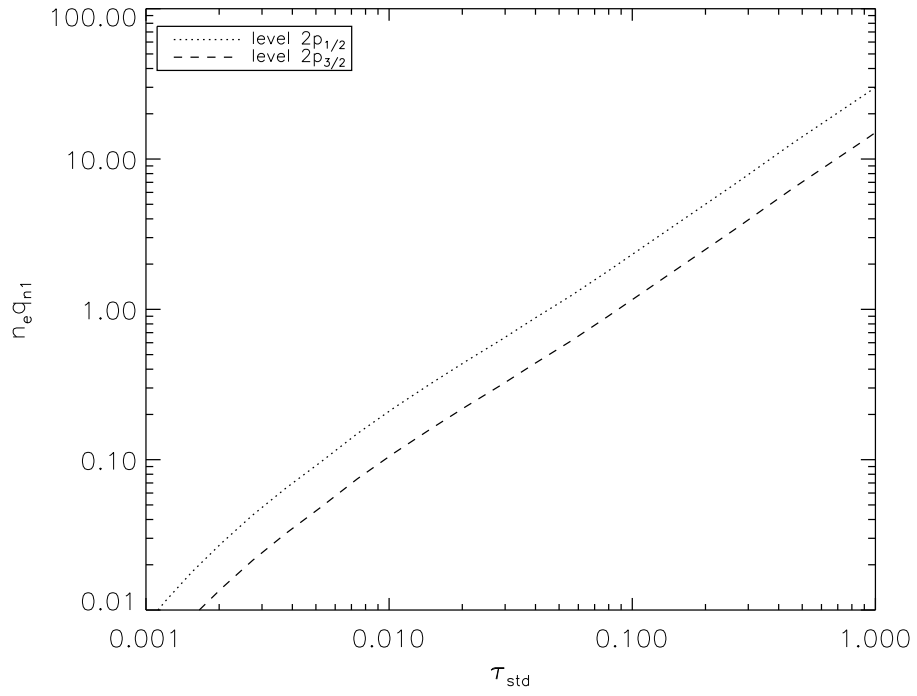


Figure 6. Collisional de-excitation coefficients of the $2p$ states versus optical depth for Model C.

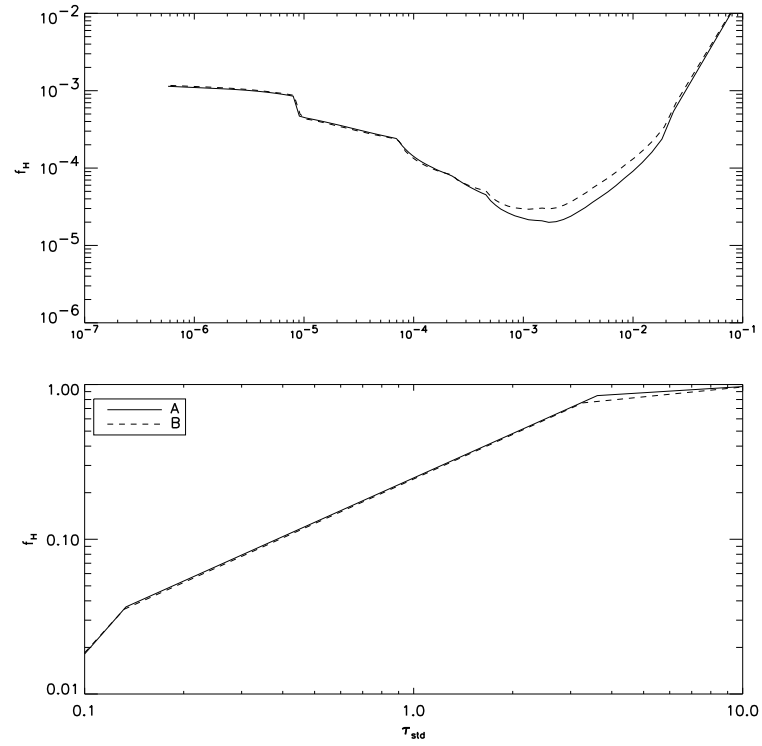


Figure 7. Comparison of hydrogen ionization fraction obtained using the 4 level (A) and the 921-level model (B) hydrogen atom in pure hydrogen under radiative equilibrium. The upper panel shows the lower optical depth regime while the lower panel shows the higher optical depth regime.

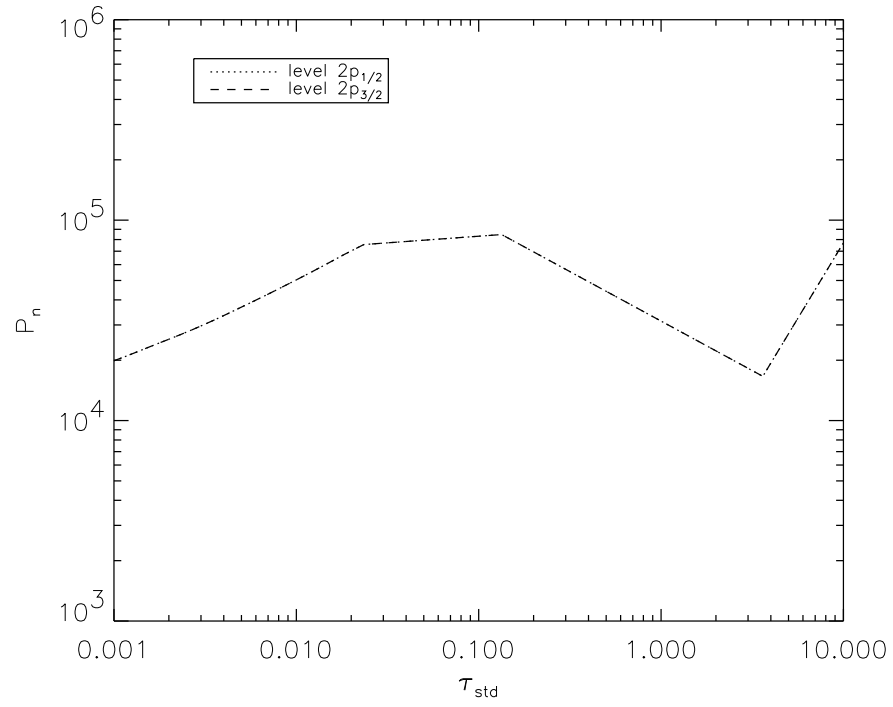


Figure 8. Photo-ionization rate versus optical depth for $2p$ states of Model A under radiative equilibrium. The last point at $\tau_{std} = 10$ is a numerical glitch caused by poor spatial resolution. The rate should continue to drop with depth.

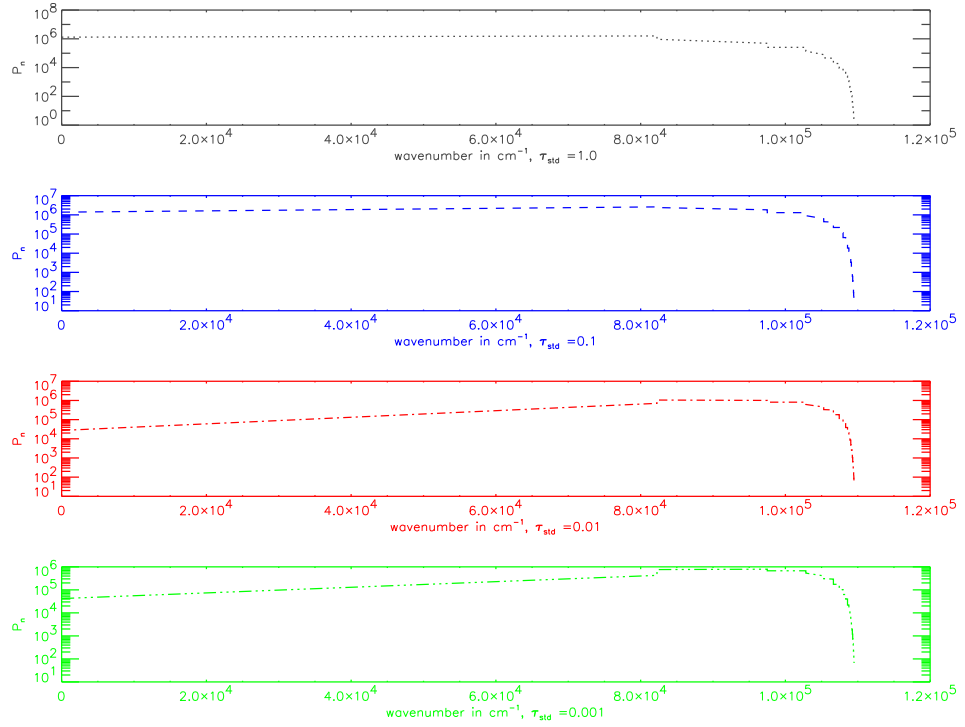


Figure 9. Photo-ionization rates versus energy level for Model B in radiative equilibrium. Each panel shows a particular optical depth.

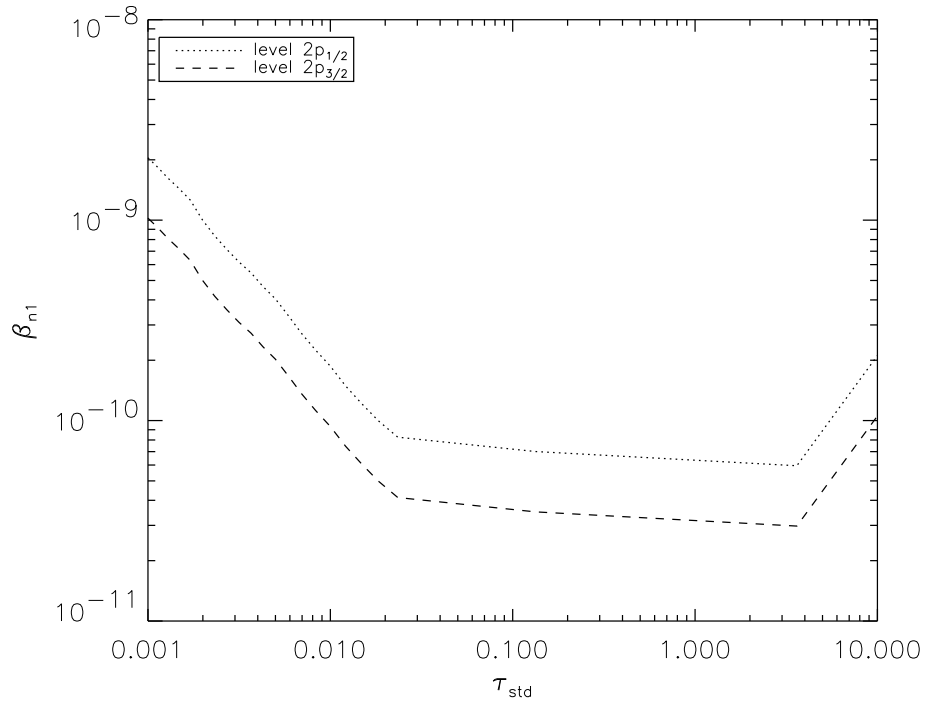


Figure 10. Escape probability versus optical depth for the $2p$ states of Model A in radiative equilibrium.

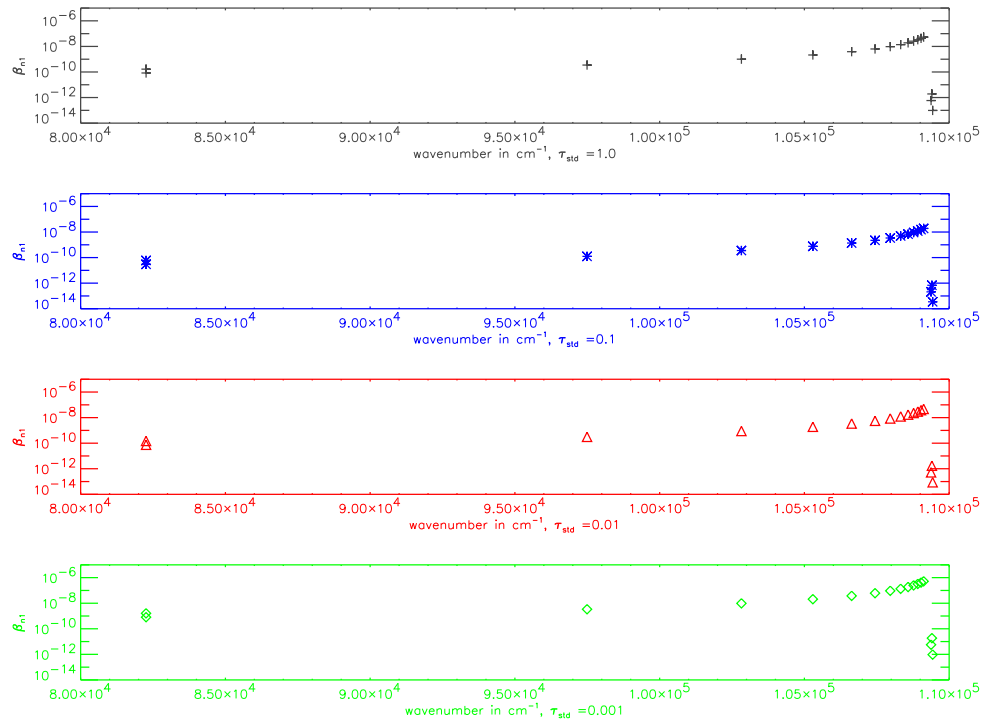


Figure 11. Escape probability versus energy level for Model B in radiative equilibrium. Each panel refers to a specific optical depth.

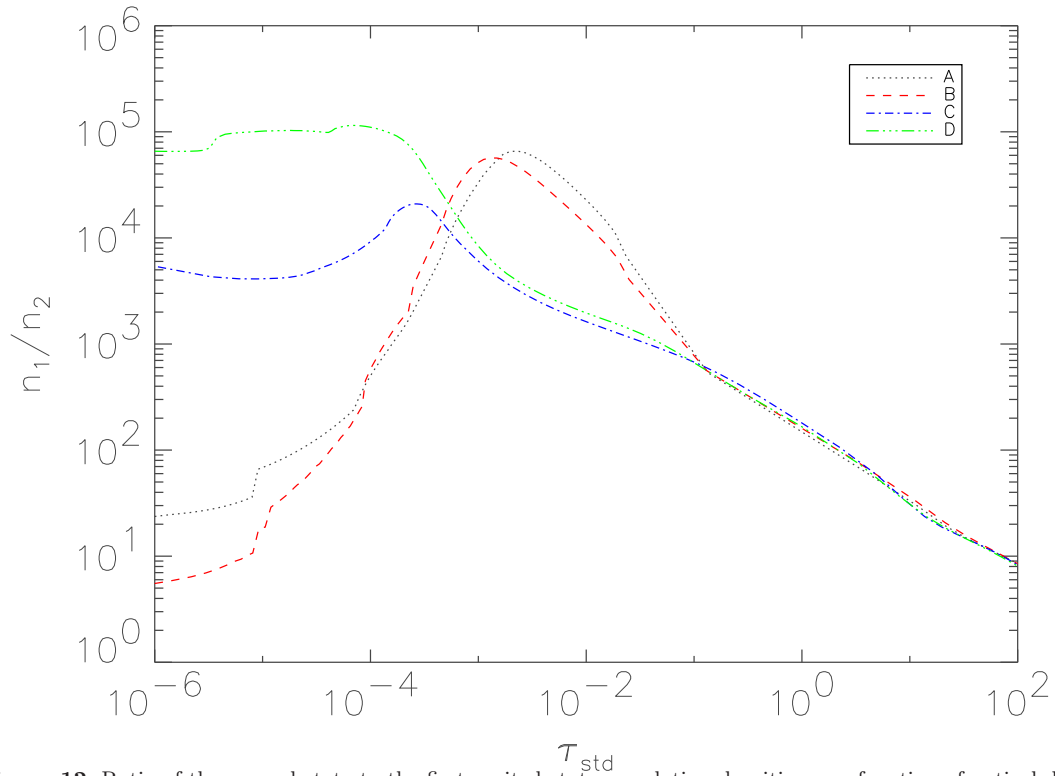


Figure 12. Ratio of the ground state to the first excited state τ_{std} population densities as a function of optical depth.